Metallophysics and Advanced Technologies
Металофіз. новітні технол.
Metallofiz. Noveishie Tekhnol.
2026, vol. 48, No. 2, pp. 123–139
https://doi.org/10.15407/mfint.48.02.0123
Reprints available directly from the publisher

PACS numbers: 52.77.Fv, 68.37.Hk, 75.50.Ww, 75.60.-d, 81.05.Bx, 81.20.Ev, 81.40.Rs

Fabrication of MnBi Magnetic Phases Using Arc-Plasma Sintering: a Novel Approach for Intermetallic Systems

Ridwan, Azwar Manaf*, Adel Fisli, Arbi Dimyati, Iwan Sumirat, Mujamilah, Ganisa Kurniati Suryaman**, and Grace Tj. Sulungbudi

Research Center for Nuclear Beam Analysis Technology,
National Research and Innovation Agency, KST B.J. Habibie Serpong,
15314 Tangerang Selatan, Indonesia
**Department of Physics, Faculty of Mathematics and Natural Sciences,*
University of Indonesia,
16424 Depok, Indonesia
***Research Center for Nuclear Material and Radioactive Waste Technology,*
KST B.J. Habibie Serpong,
15314 Tangerang Selatan, Indonesia

This study explores a novel arc-plasma sintering method for fabrication of magnetic phases in the manganese–bismuth (MnBi) alloy system with a 1:1 atomic ratio. The arc-plasma technique provides an innovative approach to sintering the intermetallic systems with elements exhibiting significantly different melting points, such as Mn (1246°C) and Bi (271.4°C). By adjusting the distance between the sample and the plasma source, temperatures up to 1250°C are rapidly reached in an argon atmosphere. Post-sintering annealing at 240°C for 4 and 24 hours influences significantly the magnetic properties of the material. Characterization is conducted using scanning electron microscopy, x-ray diffraction, and a vibrating sample magnetometer. This study highlights the potential of arc-plasma sintering as an efficient method for producing MnBi-based permanent magnets, offering a sustainable alternative to rare earth-based materials. The results demonstrate that optimiz-

Corresponding author: Ridwan
E-mail: ridw001@brin.go.id

Citation: Ridwan, Azwar Manaf, Adel Fisli, Arbi Dimyati, Iwan Sumirat, Mujamilah, Ganisa Kurniati Suryaman, and Grace Tj. Sulungbudi, Fabrication of MnBi Magnetic Phases Using Arc-Plasma Sintering: a Novel Approach for Intermetallic Systems, *Metallofiz. Noveishie Tekhnol.*, **48**, No. 2: 123–139 (2026). DOI: 10.15407/mfint.48.02.0123

ing the sintering process improves magnetic performance and enhances the structural integrity of the magnets. Further research into the microstructural transformations during annealing could provide valuable insights into the mechanisms driving these improvements.

Key words: arc-plasma sintering, MnBi, high-temperature sintering, permanent magnets, magnetic materials.

В даній роботі досліджено нову методу спікання плазмою дугового розряду для створення магнетних фаз на основі системі Манґан–Бісмут (MnBi) з атомовим співвідношенням 1:1. Плазмово-дугова методика забезпечує інноваційний підхід щодо спікання інтерметалевих систем з елементами, що мають істотно різні температури топлення, такими як Mn (1246°C) та Bi (271,4°C). Шляхом реґулювання віддалі між зразком і джерелом плазми в атмосфері арґону можна швидко досягти температури до 1250°C. Відпал після спікання за 240°C впродовж 4 і 24 годин істотно впливає на магнетні властивості матеріялу. Характеризація проводиться за допомогою сканівної електронної мікроскопії, рентґенівської дифракції та вібраційного магнетометра. Проведені дослідження демонструють потенціял методи дугового плазмового спікання як ефективної методи виробництва постійних магнетів на основі MnBi, пропонуючи стійку альтернативу матеріялам на основі рідкісноземельних елементів. Результати демонструють, що оптимізація процесу спікання поліпшує магнетні характеристики та підвищує структурну цілісність магнетів. Подальші дослідження мікроструктурних перетворень під час відпалювання можуть дати цінне розуміння механізмів, що зумовлюють ці поліпшення.

Ключові слова: дугове плазмове спікання, MnBi, високотемпературне спікання, постійні магнети, магнетні матеріяли.

(Received 26 February, 2025; in final version, 2 July, 2025)

1. INTRODUCTION

The demand for permanent magnet materials is expected to rise in response to the increasing importance of environmentally friendly energy sources in the future. Magnetic materials play a crucial role in various industries, particularly in transportation, where they are essential for replacing fossil fuels [1]. Currently, rare earth element based materials, such as NdFeB, are extensively used for permanent magnets. The demand for these materials is primarily driven by key sectors experiencing significant growth. In the electronics industry, components like motors, sensors, and actuators increasingly rely on NdFeB magnets due to the trend towards device miniaturization and improved power efficiency [1, 2]. This trend is anticipated to result in a substantial and ongoing increase in the demand for rare earth elements. However, since the production of rare earth elements is mainly concentrated in a few countries, the prices of rare-earth element-based magnetic

components are likely to continue to rise [3].

To reduce our dependence on rare earth elements, efforts are being made to obtain magnetic materials that are free of rare earth. A manganese-bismuth intermetallic alloy compound (MnBi) is a promising candidate for magnetic materials that do not contain rare earth elements and has attracted a lot of attention. This material is ferromagnetic which substantially shows anisotropic magnetocrystalline properties and has a positive coercivity coefficient temperature. This allows the material to be applied at relatively high temperatures, which are rarely found in other ferromagnetic materials [4, 5]. The permanent magnetic properties of this MnBi intermetallic system originate from the low-temperature phase (LTP) α-MnBi, which possesses a NiAs-type hexagonal crystal structure demonstrating uniaxial anisotropic magnetic properties at room temperature [6]. However, achieving a single LTP phase is challenging due to the large difference between the melting points of Mn and Bi [7]. The most used method to obtain MnBi ingots is conventional powder metallurgy. Manganese (Mn) powder is mixed with bismuth (Bi) powder in various compositions based on atomic percent and weight percent, which is then compacted and processed using arc melting methods [8], melt spinning [9, 10], or induction furnaces [11]. The resulting ingots are subsequently ground for several hours in an inert gas atmosphere [12]. The fine powder containing a magnetic phase is compacted and heat-treated in a magnetic field to enhance density and magnetic properties, with some approaches utilizing epoxy resin as a binder to produce bonded magnets [13, 14]. Other sintering methods include spark-plasma sintering [15, 16] and utilizing severe plastic deformation (SPD) techniques for bulk systems [17]. These synthesis methods are typically conducted at low temperatures, with a few publications discussing high-temperature synthesis processes. Li *et al.* [18] synthesized MnBi using an induction furnace at 900°C with directional solidification in a magnetic field, significantly enhancing crystalline anisotropy. Meanwhile, Panita Thongjumpa *et al.* [19] also obtained a ferromagnetic phase from MnBi using a microwave furnace at a temperature of 1247°C, which is slightly above the melting point of Mn.

This study presents an innovative approach to fabricating MnBi magnetic phases using arc-plasma sintering (APS). In contrast to traditional powder-based methods, APS enables the direct utilization of bulk MnBi samples, by passing the need for powderization. By achieving high temperatures rapidly within a controlled environment, this technique offers a compelling alternative to produce MnBi-based magnetic materials. The research focuses on exploring and optimizing the growth of the MnBi magnetic phase through APS, with the goal of improving both the efficiency and scalability of the fabrication process for industrial applications.

2. EXPERIMENTAL

An arc-plasma sintering facility was utilized in the synthesis process of the MnBi phase system. The plasma arc generated by the APS is highly influenced by the gas flow rate. The use of argon as a plasma gas is beneficial in creating an inert atmosphere around the material during processing, thus preventing oxygen adsorption events [20]. According to the research, the length of the plasma arc is closely related to changes in current and the flow rate of argon as the plasma gas; the temperature on the workpiece surface is directly proportional to the distance between the workpiece and the plasma source [21]. For this study, a distance of 15.5 mm between the sample and the source was maintained, with a constant current of 70 A, while the argon plasma gas flow rate was varied to 5, 6, and 7 l/min, respectively. Here, the plasma gas used is high purity argon with a flow rate of 5, 6, and 7 l/min, a fixed electric current of 70 A and a plasma life time of 10 s with a pause of 2 s with automatic settings. The working temperature of arc-plasma sintering has been verified without using a sample, with a distance between the plasma source and the empty sample container of 15.5 mm, which is equipped with a K-type thermocouple as a temperature counter. The results of temperature measurements at the sample position can be seen in Fig. 1. Based on the measurement results, it observed the plasma temperature generated is influenced by the flow rate of argon gas as the plasma gas, as it was observed by Hua Xie *et al.* [22].

The alloy used in this work with a nominal composition of $Mn_{50}Bi_{50}$ [at.%] was obtained from Xiamen Advanced High-tech Material Co.,

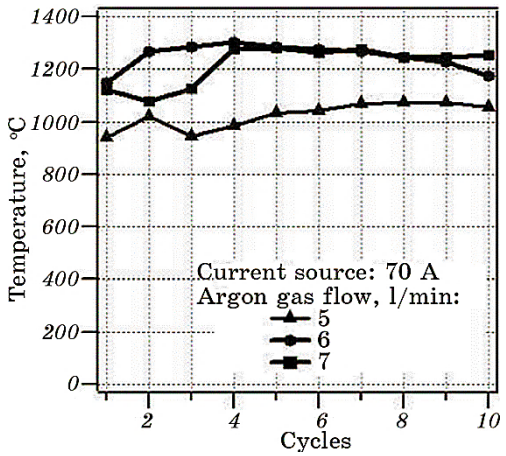

Fig. 1. The temperature of the arc plasma *versus* the plasma gas in this case high-purity argon gas.

Ltd., China. As determined by ICP, the alloy contains 20.79% wt. Mn and 78.41% wt. Bi, with a purity of 99.2%. This green alloy is a solid with a density of about 19.9 g/cm^3 and a grain size of < 250 μm. A portion of this green alloy was cut into 4 pieces with dimensions of approximately 1.0–2.0 cm^3 for the sintering and annealing processes.

The arc-plasma sintering process involved placing the sample in a graphite crucible, with a thermocouple positioned as close as possible to measure the sample temperature during sintering. Sintering was conducted at temperatures of 350°C, 1100°C (120 s/cycle), and another sample was sintered at 1100°C for 2 cycles, equivalent to 240 s of plasma 'on'. The highest sintering temperature applied in this work was 1250°C. The annealing processes were performed for all post-sintering samples at temperatures of 240°C for 4 hours and 24 hours, respectively, in a vacuum atmosphere. The sintered and annealed samples were characterized using x-ray diffraction techniques, microstructural analysis with an optical microscope and SEM equipped with EDS, and magnetic properties were measured using a vibrating sample magnetometer (VSM) at room temperature.

3. RESULTS AND DISCUSSIONS

3.1. Post Sintering and Annealed Morphology of MnBi Alloy

Figure 2 depicts the microstructure of the MnBi master alloy. The composition of the alloy, as analysed through energy-dispersive spectres-copy (EDS) and detailed in Table 1, reveals the presence of two distinct phases. The dark phase, located at point 006 in Fig. 2, *a*, is characterized by a composition of Mn 68.21 and Bi 27.32 [% wt.], which,

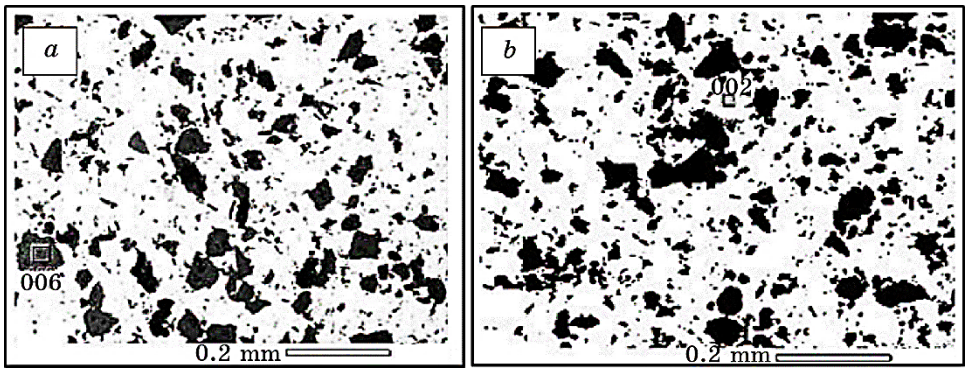

Fig. 2. The master-alloy microstructure displays the distribution of two primary phases: the dark-grey phase primarily contains the element Mn (*a*) while the white phase mostly includes the element Bi (*b*).

TABLE 1. EDS of master alloy.

Elements	Constituent elements, % wt.	
	Dark grey (marked by 006)	White (marked by 002)
Mn	68.21	9.22
Bi	27.32	86.42

based on the MnBi phase diagram, is likely to encompass both α-Mn and the intermetallic α-MnBi phases. Conversely, the light phase, identified at point 002 in Fig. 2, *b*, is primarily composed of Mn 9.22 and Bi 86.42 [% wt.].

Phase identification of the crystal structure using x-ray diffraction reveals that the master alloy does not exhibit any detectable MnBi phase within the accuracy limits of the instrument (Fig. 3). The presence of the MnBi phase in the green alloy is confirmed, though weakly, through magnetic loop measurements conducted using a vibrating sample magnetometer (VSM), as shown in Fig. 4. This can be explained by the fact that manganese (Mn), despite being adjacent to ferromagnetic elements such as iron (Fe), cobalt (Co), and nickel (Ni) in the periodic table, behaves as an antiferromagnetic material at room temperature. In contrast, bismuth (Bi) is known to be a non-magnetic material.

Figure 5 illustrates the microstructure of the alloy after sintering at 350°C, followed by annealing at 240°C for durations of 4 and 24 hours. SEM analysis reveals the microstructure of the alloy annealed for 24 hours at 240°C, as shown in Fig. 5, *a*. EDS analysis identifies the dark-coloured phase as Mn-rich and the light-coloured phase as Bi-rich.

This indicates that the alloy system has not fully formed, as evidenced by the elemental mapping results in Fig. 5, *b*, which show a distinct separation in the distribution of Mn and Bi elements rather than

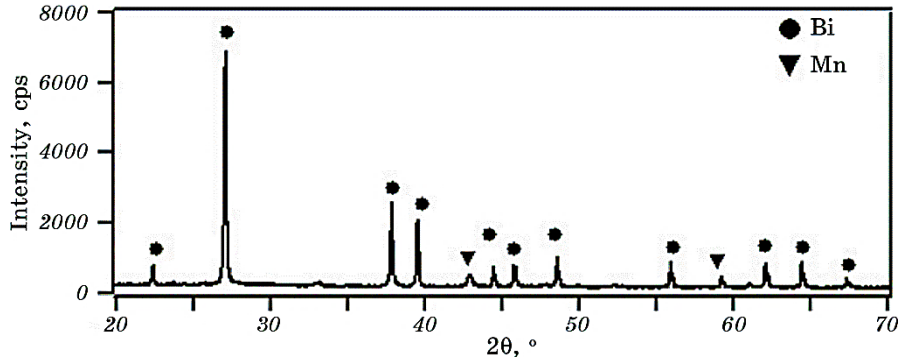

Fig. 3. The x-ray diffraction pattern of MnBi alloy confirms the presence of Mn- and Bi-rich phases.

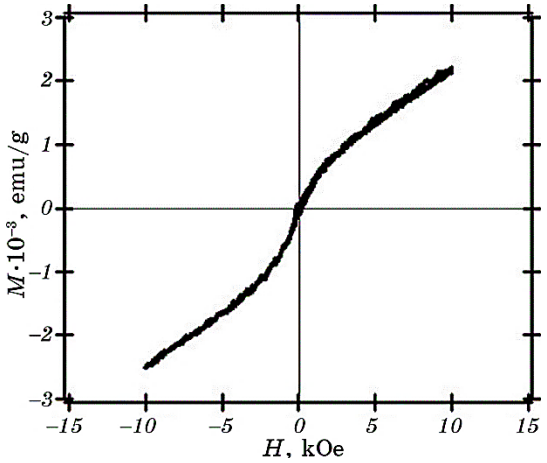

Fig. 4. The loop hysteresis of MnBi master alloy.

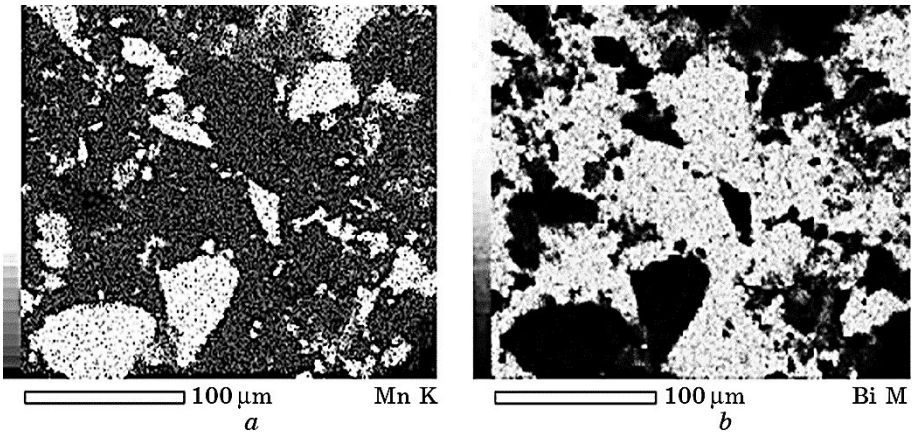

Fig. 5. Results of mapping analysis of MnBi alloy showing Mn (*a*) and Bi (*b*) elements in the microstructure.

a uniform alloy. VSM-measurement data, presented in Fig. 6, indicates that the magnetic saturation remains very low. This suggests that the low-temperature sintering process, followed by 24 hours of annealing, was insufficient to facilitate significant atomic inter-diffusion within the bulk system.

3.2. Microstructural Development during High-Temperature Sintering

Figure 7 highlights the significant microstructural transformations occurring during high-temperature sintering, specifically the for-

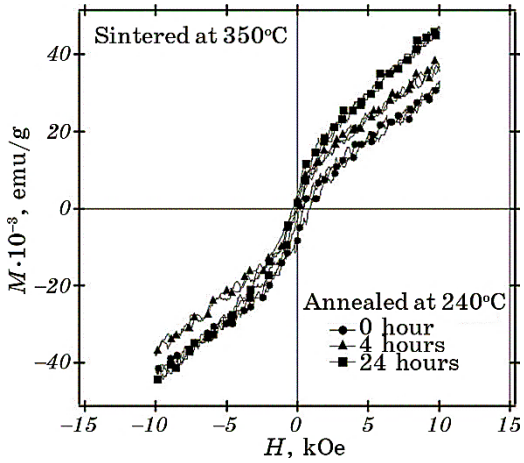

Fig. 6. Hysteresis loops of MnBi alloys annealed at 240°C for duration of 0 hour, 4 hours and 24 hours.

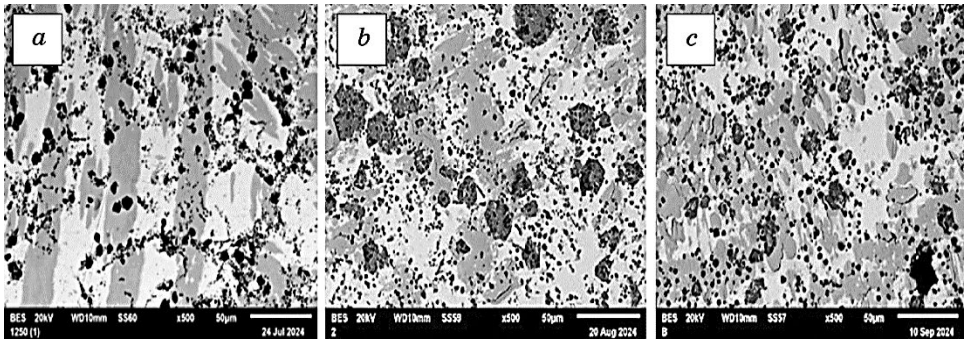

Fig. 7. SEM shows the microstructure of alloy sintered at a temperature of 1100°C for 120 s (1 cycle) before annealing (*a*) after annealing at a temperature of 240°C in a vacuum for 4 hours (*b*) and 24 hours (*c*).

mation and evolution of the MnBi phase before and after annealing.

The morphology of the MnBi phase exhibits an elongated structure, with energy dispersive spectroscopy (EDS) analysis revealing compositional shifts from Mn:Bi ratios of 24:76 [% wt.] after 4 hours of annealing to 19:81 [% wt.] after 24 hours. These changes reflect the dynamic redistribution of elements within the alloy during prolonged thermal exposure. However, due to the absence of an external magnetic field during the sintering process, the MnBi phase lacks a preferred orientation, resulting in a random arrangement. This observation underscores the potential for achieving enhanced phase alignment under an external magnetic field, as demonstrated by X. Li *et al.* [23]. The

enhanced coercivity, as determined through VSM analysis of the alloy sintered at 1100°C prior to annealing, further validates the significance of controlled processing conditions in optimizing the magnetic properties.

3.3. Role of Arc-Plasma Sintering in MnBi Phase Formation

The arc-plasma sintering technique has proven effective in facilitating the formation of the MnBi phase, despite its unique constraints. The plasma, with a brief lifetime of 10 s per cycle repeated 12 times, generates a high-temperature environment reaching 1100°C. This process enables rapid solidification and microstructural refinement. However, the surrounding Bi-rich regions have been observed to impede the growth of the MnBi phase, as noted in previous studies [10, 23]. This limitation necessitates the implementation of post-sintering annealing to promote the sustained growth of the MnBi phase.

3.4. Comparative Analysis of Magnetic Properties

Post-sintering results of MnBi alloys (50:50 composition) processed using arc-plasma techniques have demonstrated superior remanent magnetization compared to those fabricated through melt-spun ribbon methods. This distinction highlights the advantages of arc-plasma sintering in enhancing magnetic retention. However, VSM measurements conducted at room temperature under a maximum applied field of 10 kOe revealed a slight reduction in magnetic saturation following annealing at 240°C for durations of 4 and 24 hours, as compared to melt-spun ribbons [10]. Despite this, Figure 8 indicates a noticeable improvement in magnetic saturation values post-annealing, which is directly attributed to the growth of the MnBi phase. Given that MnBi is the sole ferromagnetic phase in the alloy, the observed increase in magnetic saturation strongly correlates with its enhanced development during thermal processing.

3.5. Implication for Optimization

The findings suggest that while arc-plasma sintering is effective for initiating MnBi phase formation, subsequent annealing plays a crucial role in refining the microstructure and enhancing magnetic properties. The ability to optimize the MnBi phase through controlled annealing and external magnetic field alignment represents a significant opportunity to improve further the performance of MnBi-based alloys for magnetic applications.

XRD analysis of the alloy after sintering followed by annealing at

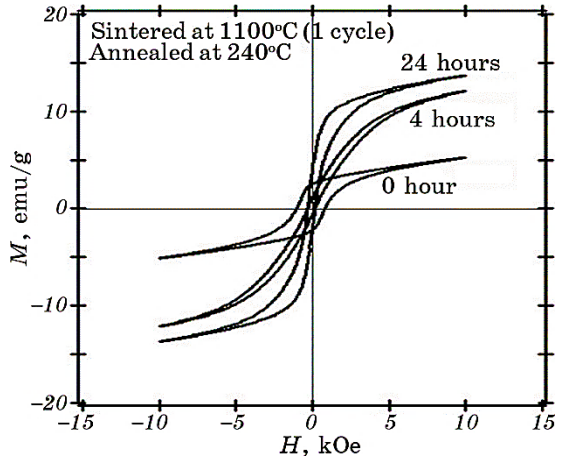

Fig. 8. Hysteresis loops of sintered at 1100°C in 1 cycle followed by annealing at 240°C for 4 hours and 24 hours in vacuum.

240°C for 4 and 24 hours detected only the presence of the Bi phase. This may be attributed to the high-temperature sintering process, which likely caused the Bi element in its liquid phase to migrate toward the surface. The diffraction peaks corresponding to the Bi phase, observed at $2\theta = 27.16°$ for the alloy annealed for 4 hours and $2\theta = 39.62°$ for the alloy annealed for 24 hours, are significantly pronounced. This suggests the potential development of texture in the material as a result of the sintering and annealing processes, as illustrated in Fig. 9.

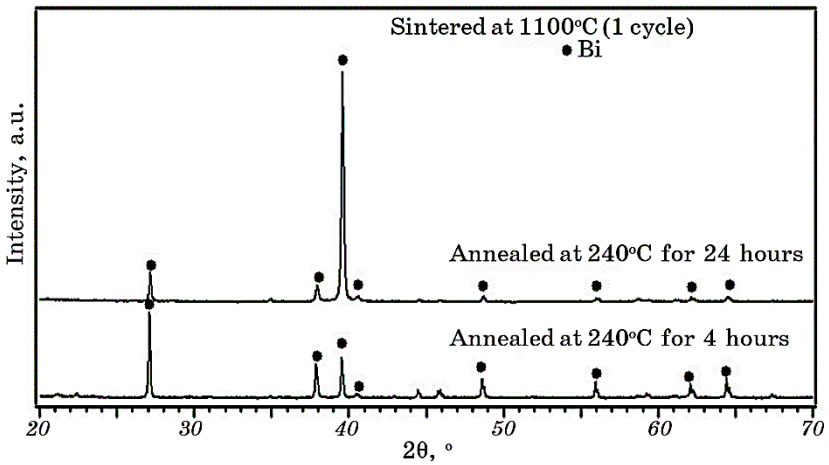

Fig. 9. The XRD pattern of the samples sintered at 1100°C in 1 cycle followed by annealing at 240°C for 4 hours and 24 hours in vacuum.

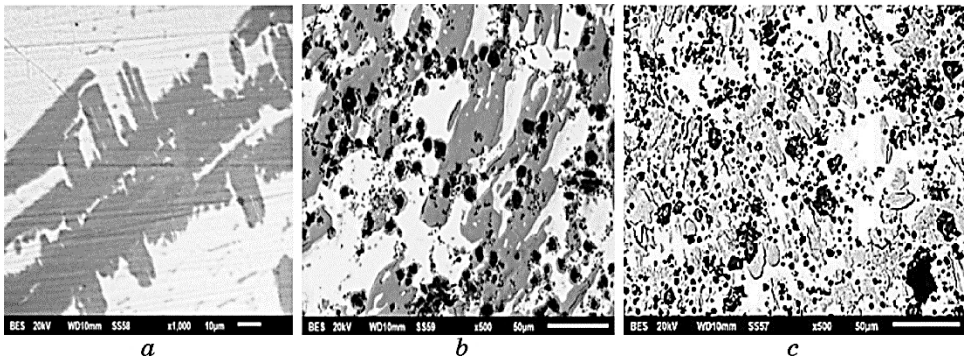

Fig. 10. The microstructure of alloy sintered at 1100°C for 240 s (2 cycles) before annealing (*a*) after annealing at 240°C in vacuum for 4 hours (*b*) and 24 hours (*c*).

When the sintering process was conducted for 240 s (2 cycles) at a temperature of 1100°C, it appeared to promote the growth of the MnBi phase, as evidenced by SEM and EDS analysis results shown in Fig. 10. The light-coloured phase remained predominantly Bi, while the dark grey phase displayed the MnBi phase with a composition of 27:73 [% wt.], and the dark-coloured phase was primarily Mn.

Following the sintering process and subsequent annealing at 240°C for 4 or 24 hours, a significant increase in magnetic saturation was observed, as illustrated in Fig. 11. Compared to the material sintered for only 1 cycle, the extended sintering duration resulted in a higher formation of the MnBi phase, as indicated by the increased magnetic satu-

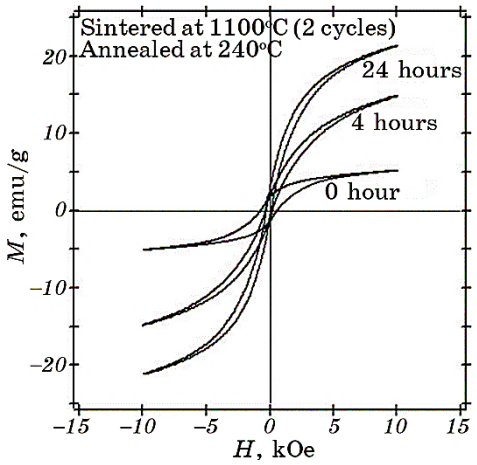

Fig. 11. The effects of sintering on the alloy MnBi, which was sintered at 1100°C for 240 s and then annealed at 240°C for 4 and 24 hours in vacuum.

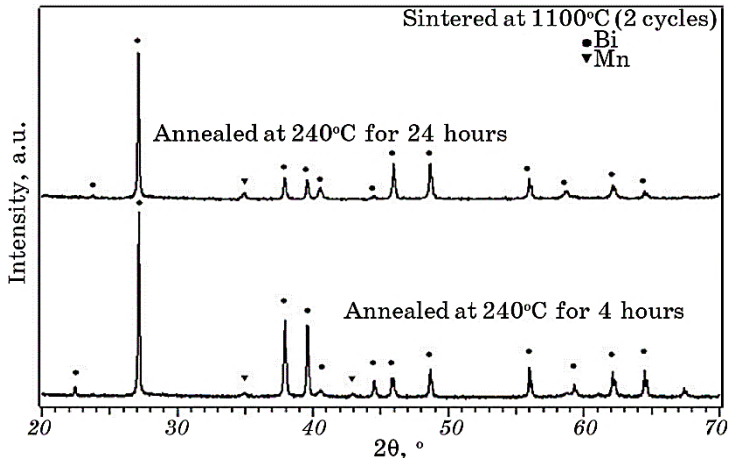

Fig. 12. XRD patterns of MnBi alloy sintered at 1100°C for 240 s, then annealed at 240°C for 4 hours and 24 hours in vacuum.

ration values. EDS analysis of the material annealed for 24 hours revealed a Mn:Bi composition of 21:79 [% wt.] in the MnBi phase. Consistent with previous XRD observations, the detected phases were still predominantly associated with the Bi phase, as shown in Fig. 12.

To gain a deeper understanding of the impact of sintering at a temperature slightly above the melting point of manganese, this study employed the arc-plasma method to sinter the MnBi alloy at 1250°C for 120 s (1 cycle). This high-temperature approach aims to investigate its role in promoting phase growth and improving material properties. SEM analysis provides clear evidence that the MnBi phase (represented by the dark grey regions) exhibits significantly larger grain sizes compared to its formation during the solidification process, as highlighted in Fig. 13. The increased grain size indicates enhanced phase development, which is essential for optimizing the magnetic properties of the material.

Further insights were gathered from magnetic hysteresis curve measurements, which revealed a noticeable decrease in coercivity after sintering at 1250°C. This reduction is likely attributed to the intensive growth of the MnBi phase, with grain sizes surpassing 50 μm [24]. Despite this decrease in coercivity, the remanence value of the annealed material was observed to be comparable to that of material sintered at 1100°C, suggesting that the remanent magnetization remains stable across the two sintering conditions. This stability in remanence, coupled with the enhanced MnBi phase formation, highlights the effectiveness of sintering at 1250°C in promoting phase growth without compromising key magnetic properties.

A closer examination of Fig. 13 further underscores the structural

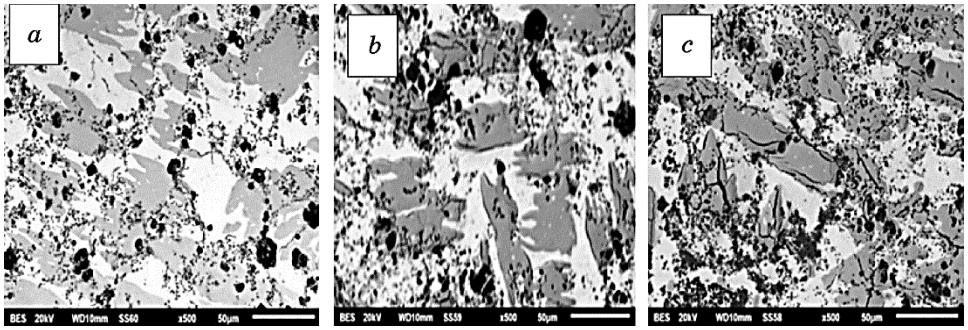

Fig. 13. The microstructure sintered at 1250°C (1 cycle) before annealing (*a*) after annealing at 240°C in a vacuum for 4 hours (*b*) and 24 hours (*c*).

benefits of the elevated sintering temperature. The MnBi phase grains are not only densely distributed throughout the alloy but also show signs of fusion, indicating a high degree of interconnectivity. This dense and cohesive grain distribution likely contributes to the improved structural integrity and magnetic uniformity of the material. Overall, the findings suggest that sintering at 1250°C is a promising strategy for enhancing the MnBi phase while maintaining the magnetic and structural performance required for advanced applications.

With the presence of heat, this will support the occurrence of diffusion reactions at the grain boundaries, which will then generate the formation of the MnBi phase. The grain boundary was partially melted by reaction heat, inducing the growth of the reactant. Since there are some eutectic melting states at the boundary, this is considered similar to the semi-solid melting state [25]. Although the melted area was small, the formed ferromagnetic grain can move in the melted area, resulting in the closeness of the ferromagnetic grain.

As seen in Figure 14, magnetic saturation grows monotonically with annealing time. This is further verified by the x-ray diffraction data of MnBi alloy after sintering at 1250°C and followed by annealing procedure at 240°C for 4 and 24 hours respectively, where the MnBi phase can be clearly detected, as shown in Fig. 15. The x-ray diffraction (XRD) data analysis, depicted in Figs. 9 and 12, indicates that bismuth is the predominant phase present in the system. This observation can be attributed to the significantly higher atomic number of bismuth, $Z = 83$, compared to manganese's $Z = 25$. Moreover, the elevated sintering temperature utilized in this study surpasses the melting point of bismuth, facilitating the migration of bismuth atoms towards the alloy's surface during the cooling stage. This process is expected to lead to the accumulation of bismuth-rich phases on the surface [26]. Additionally, the utilization of bulk materials in the sintering and annealing processes in this study may account for the predominant detection

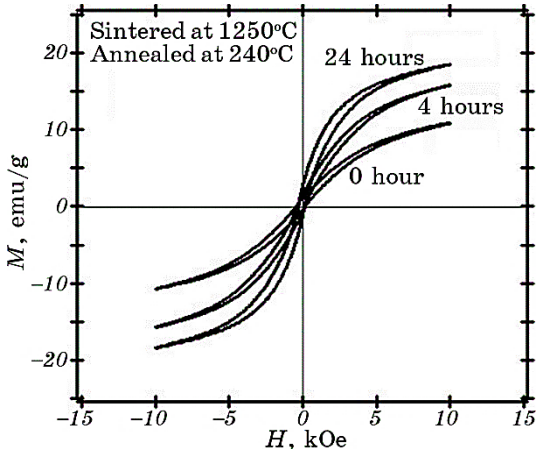

Fig. 14. The effects of sintering the MnBi alloy at 1250°C are presented, along with the subsequent annealing process conducted in a vacuum at 240°C for both 4 and 24 hours.

of Bi diffraction patterns. It was only at a sintering temperature of 1250°C that the α-MnBi phase was distinctly observed, as seen in Fig. 15. With the sintering temperature exceeding the manganese melting point, the higher temperature offers advantages for the precipitation reaction between Mn and Bi.

Based on the VSM-measurement results, it is shown that the coercivity of MnBi after the sintering process in this study is consistently

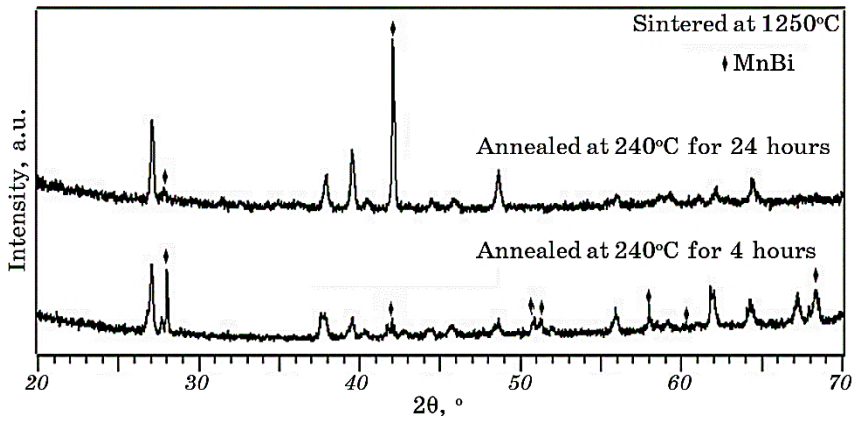

Fig. 15. The XRD pattern of the MnBi alloy, which was sintered at 1250°C and subsequently annealed in a vacuum at 240°C for durations of 4 hours and 24 hours, is presented. This analysis indicates the presence of the α-MnBi phase, while the unmarked peaks correspond to other phases, specifically, Bi or Mn.

greater than that after annealing, as seen in Fig. 14. Since magnetic coercivity is significantly influenced by complex microstructural conditions, the magnetic phase resulting from the sintering process in this case is likely isolated from other non-ferromagnetic phases like Mn, Bi, or MnO that form during the solidification of the liquid phase.

Conversely, during the annealing process, interdiffusion takes place, leading to the development of a ferromagnetic phase characterized by in-creased remanence but decreased coercivity, aligning with the findings of J. Cao *et al.* [26] on the impact of the intergranular phase on the magnetic properties of the MnBi system. Therefore, it is well documented that to boost the magnetic coercivity of the MnBi system, grinding using the ball milling method followed by an extended annealing process is crucial. Ongoing research focusing on the production of α-MnBi through the arc-plasma sintering technique followed by milling is underway, with the outcomes to be detailed in future publications.

4. CONCLUSIONS

This study demonstrates the viability of utilizing arc-plasma sintering as an alternative method for forming the ferromagnetic MnBi phase. The results highlight that the growth and formation of the MnBi phase are highly dependent on the sintering temperature and duration, with higher temperatures and extended sintering times promoting more extensive phase development. Post-annealing, the observed increase in magnetic remanence further confirms the enhancement of the ferromagnetic MnBi phase.

Even in the absence of an applied magnetic field during the sintering and annealing processes, XRD analysis indicates that the MnBi phase elongates at sintering temperatures exceeding 1100°C. This suggests that the method intrinsically supports the structural alignment necessary for improved magnetic properties.

The use of the arc-plasma technique not only allows precise control over the sintering parameters but also opens the potential for conducting the sintering process in the presence of an external magnetic field. This could further promote magnetocrystalline anisotropy, paving the way for the efficient production of rare-earth free hard magnetic bulk materials. These findings underscore the promise of arc-plasma sintering as a scalable and innovative approach for developing advanced magnetic materials.

This research activity is supported through RIIM Kompetisi funding from the Indonesia Endowment Fund for Education Agency, Ministry of Finance of the Republic of Indonesia and National Research and Innovation Agency of Indonesia according to the contract number: B-1932/III.2/FR 06.01/7/2023. We also thank the Nuclear Energy

Research Organization/Research Center for Neutron Beam Analysis Technology–National Research and Innovation Agency of Indonesia and department of Physics, Faculty of Mathematics and Natural Sciences, University of Indonesia for supporting these research activities.

AUTHORS' CONTRIBUTIONS

Ridwan, designed the project activities, collected and reviewed the literature, and performed x-ray diffraction data analysis, supervised the measurement data and wrote the manuscript based on input from other authors. Azwar Manaf has analysed the SEM–EDS data and reviewed the draft manuscript carefully and in detail and has provided very useful input for improving the manuscript, Adel Fisli has analysed the phase changes of the material related to the results of the heat treatment process, Arbi Dimyati supervised the use of APS facilities so that the project can run well, Iwan Sumirat reviewed the manuscript and provided input for improving the manuscript, Mujamilah collected magnetic data and along with the initial analysis, Ganisa Kurniati Suryaman collected annealing data in a noble gas atmosphere and along with the initial analysis of the results of the heat treatment process, Grace Tj. Sulungbudi collected SEM–EDS data and helped with the initial interpretation. After discussing and reviewing the manuscript as a whole, all authors have approved the final version of this manuscript.

REFERENCES

1. M. J. Kramer, R. W. McCallum, I. A. Anderson, and S. Constantinides, *JOM*, **64**: 752 (2012).
2. O. Gutfleisch, M. A. Willard, E. Brück, C. H. Chen, S. G. Sankar, and J. P. Liu, *Adv. Mater.*, **23**, Iss. 7: 821(2011).
3. X. Du and T. E. Graedel, *J. Ind. Ecol.*, **15**, Iss. 6: 836 (2011).
4. Y. B. Yang, X. G. Chen, R. Wu, J. Z. Wei, X. B. Ma, J. Z. Han, H. L. Du, S. Q. Liu, C. S. Wang, Y. C. Yang, Y. Zhang, and J. B. Yang, *J. Appl. Phys.*, **111**, Iss. 7: 30 (2012).
5. N. V. Rama Rao, A. M. Gabay, W. F. Li, and G. C. Hadjipanayis, *J. Phys. D: Appl. Phys.*, **46**: 265001 (2013).
6. N. Van Vuong, *Communications Phys.*, **29**, No. 4: 441 (2019).
7. A. Sarkar and A. Basu Mallick, *JOM*, **72**: 2812 (2020).
8. W. Xie, E. Polikarpov, J. P. Choi, M. E. Bowden, K. Sun, and J. Cui, *J. Alloys Compd.*, **680**: 1 (2016).
9. S. Kim, H. Moon, H. Jung, S.-M. Kim, H.-S. Lee, H. Choi-Yim, and W. Lee, *J. Alloys Compd.*, **708**: 1245 (2017).
10. T. Saito, R. Nishimura, and D. Nishio-Hamane, *J. Magn. Magn. Mater.*, **349**: 9 (2014).
11. Y. Yang, J. Park, J. T. Lim, J. W. Kim, O. L. Li, and C. J. Choi, *J. Magn. Magn. Mater.*, **517**: 167344 (2020).

12. C. Li, Y. Yang, S. Lu, Z. Xiang, L. Chen, N. X. Truong, H. Xu, and W. Lu, *Mater. Res. Express*, **11**: 016520 (2024).
13. J. B. Yang, K. Kamaraju, W. B. Yelon, W. J. James, Q. Cai, and A. Bollero, *Appl. Phys. Lett.*, **79**, Iss. 12: 1846 (2001).
14. D.-T. Zhang, P.-F. Wang, M. Yue, W.-Q. Liu, J.-X. Zhang, J. A. Sundararajan, and Y. Qiang, *Rare Metals*, **35**: 471 (2016).
15. K. Y. Ko, S. J. Choi, S. K. Yoon, and Y. S. Kwon, *J. Magn. Magn. Mater.*, **310**, Iss. 2, Pt. 3: e887 (2007).
16. O. Guillon, J. G. Julian, B. Dargatz, T. Kessel, G. Schierning, J. Räthel and M. Herrmann, *Adv. Eng. Mater.*, **16**, Iss. 7: 830 (2014).
17. L. Weissitsch, S. Wurster, H. Krenn, and A. Bachmaier, *Mater. Res. Lett.*, **12**, Iss. 3: 226 (2024).
18. X. Li, Y. Fautrelle, and Z. Ren, *Acta Mater.*, **55**, Iss. 16: 5333 (2007).
19. P. Thongjumpa, T. Charoensuk, U. Boonyang, P. Harding, and C. Sirisathitkul, *J. Cent. South Univ.*, **27**: 2220 (2020).
20. P. Fauchais and A. Vardelle, *IEEE Trans. Plasma Sci.*, **25**, Iss. 6: 1258 (1997).
21. T. Iwao and T. Inaba, *Vacuum*, **65**, Iss. 3–4: 299 (2002).
22. H. Xie, N. Liu, Q. Zhang, H. Zhong, L. Guo, X. Zhao, D. Li, S. Liu, Z. Huang, A. D. Lele, A. H. Brozena, X. Wang, K. Song, S. Chen, Y. Yao, M. Chi, W. Xiong, J. Rao, M. Zhao, M. N. Shneider, J. Luo, J.-C. Zhao, Y. Ju, and L. Hu, *Nature*, **623**: 964 (2023).
23. J. Zamora, I. Betancourt, and I. A. Figueroa, *Revista Mexicana de Física*, **64**, No. 2: 141 (2018).
24. J. Zamora, I. Betancourt, and I. A. Figueroa, *J. Supercond. Nov. Magn.*, **31**: 873 (2018).
25. P. Heitjans and J. Kärger, *Diffusion in Condensed Matter: Methods, Materials, Models* (Heidelberg: Springer: 2005).
26. J. Cao, Y. L. Huang, Y. H. Hou, G. Q. Zhang, Z. Q. Shi, Z. C. Zhong, and Z. W. Liu, *AIP Adv.*, **8**: 055132 (2018).